Wind and Structures, *Vol. 16, No. 6 (2013) 579-601*
DOI:http://dx.doi.org/10.12989/was.2013.16.6.579

Influence of latitude wind pressure distribution on the responses of hyperbolodial cooling tower shell

Jun-Feng Zhang[1,2], Yao-Jun Ge[*2] and Lin Zhao[2]

[1]*School of Civil Engineering, Zhengzhou University, Zhengzhou 450001, China*
[2]*State Key Laboratory for Disaster Reduction in Civil Engineering, Tongji University, Shanghai 200092, China*

(Received March 25, 2012, Revised June 16, 2012, Accepted July 7, 2012)

Abstract. Interference effects are of considerable concern for group hyperboloidal cooling towers, but evaluation methods and results are different from each other because of the insufficient understanding on the structure behavior. Therefore, the mechanical performance of hyperboloidal cooling tower shell under wind loads was illustrated according to some basic properties drawn from horizontal rings and cantilever beams. The hyperboloidal cooling tower shell can be regarded as the coupling of horizontal rings and meridian cantilever beams, and this perception is beneficial for understanding the mechanical performance under wind loads. Afterwards, the mean external latitude wind pressure distribution, $C_P(\theta)$, was artificially adjusted to pursue the relationship between different $C_P(\theta)$ and wind-induced responses. It was found that the maximum responses in hyperboloidal cooling tower shell are primarily dominated by the non-uniformity of $C_P(\theta)$ but not the local pressure amplitude C_P or overall resistance/drag coefficient C_D. In all the internal forces, the maximum amplitude of meridian axial tension shows remarkable sensitivity to the variation of $C_P(\theta)$ and it's also the controlling force in structure design, so it was selected as an indicator to evaluate the influence of $C_P(\theta)$ on responses. Based on its sensitivity to different adjustment parameters of $C_P(\theta)$, an comprehensive response influence factor, *RIF*, was deduced to assess the meridian axial tension for arbitrary $C_P(\theta)$.

Keywords: hyperboloidal cooling towers; latitude wind pressure distribution; mechanical performance; evaluation indicator; response influence factor

1. Introduction

As the largest reinforced concrete thin-shelled structures, hyperboloidal cooling towers (HCTs) are governed by wind loads in structure design and attract many attentions in wind engineering. Wind engineering research on hyperboloidal cooling towers focus on internal and external wind pressure distribution (Armitt 1980, Niemann 1980, Sun and Zhou 1983, Zhao and Ge 2010), wind-excited responses (Armitt 1980, Niemann 1980, Zhao and Ge 2010), group tower interference effects (Armitt 1980, Niemann and Köpper 1998, Orlando 2001, Zhao and Ge 2010), ultimate load bearing capacity (Mang *et al.* 1986, Noh 2005, Gopinath *et al.* 2012) and the stability problems induced by wind (Abel *et al.* 1982, Andres and Harte 2006, Sabouri-Ghomi *et al.* 2006), among which the mean external latitude wind pressure distribution $C_P(\theta)$ is the basis of wind loads

*Corresponding author, Professor, E-mail: yaojunge@tongji.edu.cn

http://www.techno-press.org/?journal=was&subpage=8 ISSN: 1226-6116 (Print), 1598-6225 (Online)

for structure design, and the HCT shell's internal forces are extremely sensitive to $C_P(\theta)$ (Armitt 1980). Due to the complexity of the problem itself, $C_P(\theta)$ from full-scale measurements are limited and different to some extent (Sun and Zhou 1983) (Fig. 1 (a)) owning to the influence of site topography, with or without ribs, surrounding buildings, weather conditions, methods of measurements and data analyses and so on (Armitt 1980, Niemann 1980). $C_P(\theta)$ from wind tunnel tests and numerical simulations show even greater discrepancy because of the Reynolds number effects. Similarly, $C_P(\theta)$ given by different scholars and codes are different from each other (Fig. 1 (b)). As circular cross-section structures, the $C_P(\theta)$ of HCTs can be divided into three regions, namely windward (WW), sideward (SW) and leeward (LW), and differences are mainly in the sideward and leeward regions among different sources. Different wind pressure distributions will get different responses, but the relationship between them is still not clear.

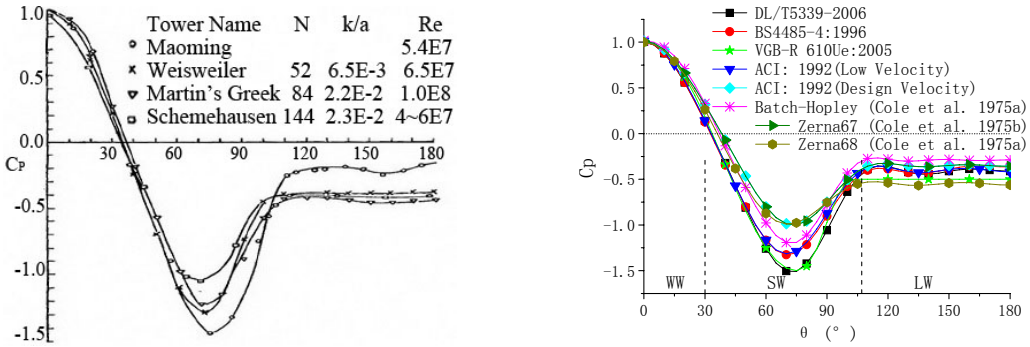

(a) full-scale measurements (b) codes and scholars

Fig. 1 Wind pressure distributions from different resources

Moreover, wind pressure in all the three regions may be affected by the interference effects of surrounding buildings and HCTs, and researches targeting at the interference effects are always initiated for loads and responses separately. The former focuses on $C_P(\theta)$ itself (Armitt 1980, Orlando 2001) or the overall resistance/drag coefficient C_D (Zhao and Ge 2010). For the latter there are two methods: the direct method, using continuous medium (Niemann and Köpper 1998) or equivalent beam-net (Zhao and Ge 2010) aeroelastic models and taking the stresses or displacements as indicators to evaluate the interference effects; and the indirect method, using different wind pressure distributions obtained from the rigid model tests to calculate the corresponding responses and then the interference effects would be obtained with certain responses as evaluation indicators (Orlando 2001).

For practical and straightforward design process, the typical $C_P(\theta)$ from single tower is always multiplied by interference effects magnification factor (Interference Factor, *IF*) for group towers, but not the interfered $C_P(\theta)$. However, the methods and values for *IF* are different in different researches and codes. Just like in high-rise buildings, local pressure amplitude C_P at certain location is always used as the evaluation indicator (Orlando 2001, John 2011). In Chinese codes (DL/T 5339-2006), there is no explicit regulation for *IF*, and *IF* is always determined with the indicator of C_D through rigid model tests which is also widely used in high-rise buildings. In both British and German codes (BS 4485 1996, VGB-R 610Ue 2005), *IF* is given with the indicator of

meridian tensile stresses directly got from continuous medium aeroelastic model tests, but their methods and values for *IF* are also different. Actually, the interference effects originate from the change of wind pressure distribution, and the selected evaluation indicator for interference effects will not be reasonable if the relationship between wind pressure distribution and responses is not fully understood.

Additionally, the mechanical performance of HCT should also be included in the interference effects research. For example, for rectangular high-rise buildings, wind pressure in sideward has little influence on the along-wind responses and, approximately, the wind pressure in windward and leeward are both uniform so can be regarded as line loads. Therefore, C_D is a direct indicator of the overall along-wind action. Also, the existence of rigid diaphragms makes it certain that the responses in vertical structure members are directly related to the C_D, such as the axial force and shear force in columns and the moment and shear force in shear walls. On the other hand, local pressure amplitude C_P is directly related to the responses in building envelops. As a consequence, it's reasonable to take C_D or C_P as an indicator for interference effects of high-rise buildings according to different application purpose.

However, HCTs and high-rise buildings are different from each other not only in structure behavior but also in wind loads. Wind loads on HCTs is three-dimensional surface pressure and the pressure variation at any point will give influences on load effects in the whole shell, which means the variation of local pressure amplitude C_P will not be directly related to the concerned response. Additionally, different $C_P(\theta)$ will have the same C_D for HCTs just like circular columns, but the responses will be quite different. Therefore, for HCTs, the evaluation indicator and evaluation method for wind-induced responses should be determined based on the mechanical performance of HCTs themselves and the relationship between wind pressure distribution and responses. Aeroelastic model tests or calculation can get the wind-induced responses, but they just target at the responses or interference effects, rather than the mechanical performance of HCTs under wind loads or the relationship between $C_P(\theta)$ and responses. On the other hand, what are concerned primarily in structure design are the maximum internal forces yet the structure behavior is ignored always, so that stress states rather than loads are used in local buckling approach owing to the insufficient knowledge on mechanical performance under wind loads (Mungan 1982).

Continually higher and larger HCTs always in group set are constantly needed in power plants for economic and environmental benefits, and the interference effects are different from case to case. Although aeroelastic model tests can get the interference effects directly, the costs in time and money are quite huge so that can't be applied for all plants. Rigid model tests are easy but neither C_D nor C_P can be used for interference effects. So, it's demanded to investigate the relationship between wind pressure distribution and responses based on the mechanical performance of HCTs, from which the interference effects can be obtained just from rigid model tests. Although the dynamic effects of wind loads can't be ignored, yet the study should be started from the static wind loads and wind-induced responses.

For the reasons above, the mean external latitude wind pressure distribution $C_P(\theta)$ from Chinese code (DL/T 5339-2006) is artificially adjusted and the corresponding responses are analyzed, taking four cooling tower as examples (Table 1). According to Fig. 1 and previous experiments, the adjust including four parameters: wind pressure amplitude in windward, sideward and leeward regions and also the location of minimum point of $C_P(\theta)$ ($C_{P,\,min}$). Consequently, the mechanism of influence of $C_P(\theta)$ on wind load effects was obtained which is meaningful for interference effects research. What should be noted is that the inner pressure is not included in $C_P(\theta)$ because it's always uniform along the latitude. For convenience, ring structures under

circular pressure were adopted to illustrate the mechanical performance of HCTs under wind loads analogously.

Table 1 Parameters of cooling towers and related wind properties

Tower Name	Unit: m, T_0 is the thickness at throat, other parameters can be found in Fig. 2									f_{min} (Hz)	V_0 (m/s)
	Z_H	Z_T	Z_S	Z_B	R_B	R_S	R_T	R_H	T_0		
TSPL in India	155.002	118.801	10.6	-0.254	60.355	57.128	34.357	36.666	0.275	1.06	33.8
Pengcheng in China	166.96	130.17	11.5	-0.5	66.297	63.12	38.506	40.523	0.22	0.81	24.0
Ninghai in China	177.146	141.133	12.216	-0.1536	71.4436	67.347	39.108	39.86	0.271	0.93	31.0
Wuhu in China	183.89	138.377	12.4	1.952	73.349	69.978	40.571	43.5015	0.24	0.75	24.0

Note: According to DL/T 5339-2006, V_0 is the basic wind speed which corresponds to the 50-year-recurrence 10-minute mean wind speed in Exposure B at an elevation of 10m. For all the four towers, their exposure categories are all the Exposure B, which mean that the mean wind speed power law factor is α=0.16.

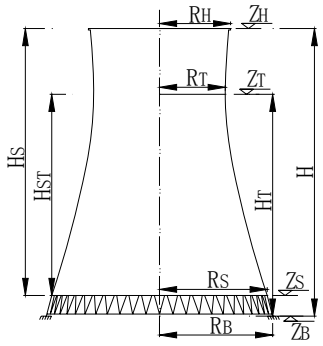

Fig. 2 Definitions for the dimensions of cooling towers

2. Mechanical performance under wind loads

The height and diameter of HCTs are close to each other, always Z_H/D_T<2.5, and the mode shapes of HCTs can be regarded as the coupling of mode shapes of horizontal rings supported elastically at top and bottom edges and meridian cantilever beams supported elastically in right and left sides. Moreover, the mechanical performance of HCTs under mean wind loads reflects both that of the horizontal rings and cantilever beams. For example, the shell's displacement under three-dimensional wind loads is reflected in the latitude deformation of horizontal rings and also in the lateral bending of meridian cantilever beams. Another, $C_P(\theta)$ of HCTs can also be separated into two parts (Fig. 3): the uniform part $C_{P,U}(\theta)$=-0.39 and the nonuniform part $C_{P,N}(\theta)$. $C_{P,N}(\theta)$ is

similar to $O_{rth}(\theta)$, which is the union of tension in one direction and compression in the perpendicular direction, but with the leeward push missed. $C_{P,U}(\theta)$ and $O_{rth}(\theta)$ are both common loads for rings so it will be analyzed firstly.

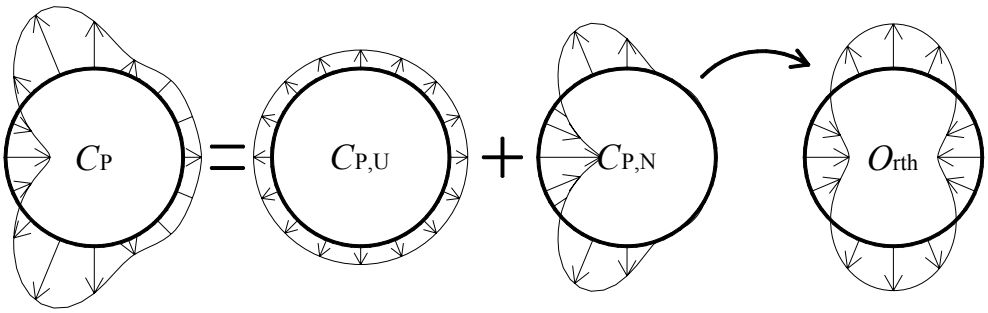

Fig. 3 Decomposition of latitude wind pressure distribution

2.1 Structure behavior of thin-walled ring structures

For thin-walled ring structures, their deformation and internal forces distributions are both in close relations to the circular pressure distribution and must meet the circular deformation compatibility condition because they are enclosed structures. Obviously, their deformation will be the slightest under $C_{P,U}(\theta)$ but the most dramatic under $O_{rth}(\theta)$. Because there is merely uniform latitude axial force but no moment in the former case, the shape of the rings is still circular yet the perimeter changes. In the latter case, however, latitude axial force and moment are both nonuniform, so the rings can't sustain their origin shapes and the deformation consistent with the circular pressure distribution appears. Also, the maxima and minima of latitude axial force and moment all locate at the peak points of circular pressure (Fig. 4). The meanings of symbols in Fig. 4 list below

$$F_i = f_i \times P_i R;\ \ M_i = m_i \times P_i R^2;\ \ U_i = u_i \times P_i R^4 / EI \tag{1}$$

in which, P_i, F_i, M_i, U_i are the circular pressure, axial force, moment, displacement at point A or B; f_i, m_i, u_i are the corresponding calculation factors. The pressure is positive for compression, the axial force is positive for tension, the moment is positive if external surface is tension, and the displacement is positive for inward. Obviously, the section's bending stiffness (EI) is much smaller than the axial stiffness (EA) for thin-walled structures, so the controlling indicators in structure design under $O_{rth}(\theta)$ would be the deformation and moment but not the axial force.

Moreover, even if the rings are just under uniaxial tension or uniaxial compression in single direction, opposite deformation in the perpendicular direction will be observed as well because of the deformation compatibility condition. As a result, the tension in one direction and the compression in the perpendicular direction will be assistants for each other, which aggravates the deformation. Therefore, the two controlling indicators in structure design, the deformation and moment, are both related to the non-uniformity of circular pressure distribution (Fig. 5). The

non-uniformity can be expressed by the pressure difference between point A and B (i.e., P_A-P_B), because there are just two perpendicular crests and hollows for the circular pressure.

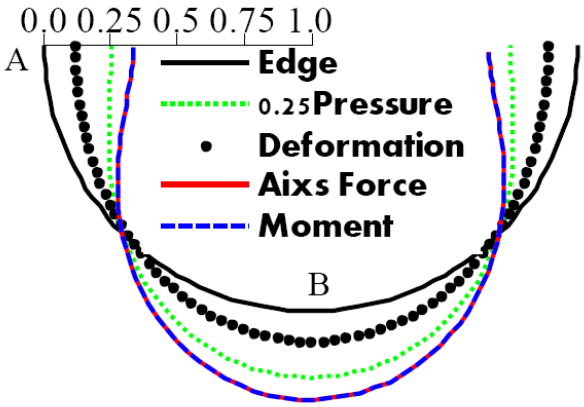

Fig. 4 Distribution of load and load effects of rings

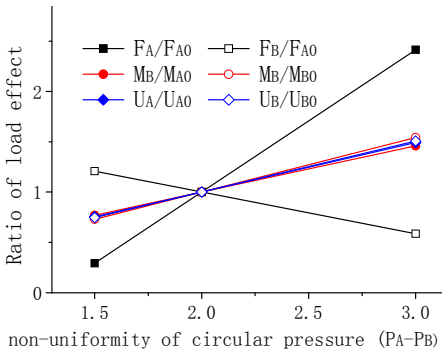

Fig. 5 Influence of load uniformity on load effects

2.2 Mechanical performance of HCTs under wind loads

For HCTs under the bilateral symmetrical wind loads, the latitude deformation varies with height but can be divided into four areas for the whole height. Area I, II and IV correspond to windward, sideward and leeward region of $C_P(\theta)$ respectively (Fig. 1, Fig. 6 (a)). An additional one, area III, which covers the adjacent area of sideward and leeward regions is separated especially because the latitude deformation there is inconsistent with the wind pressure distribution in this scope.

Deformation in area I is inward for the push of windward pressure ($C_{P,WW}$) and in area II is outward for the suction of sideward pressure ($C_{P,SW}$). Wind pressure in area I is also contributive to the deformation in area II and vice versa, which is similar to the rings under $O_{rth}(\theta)$. Furthermore,

the deformation patterns in area I and II are almost the same for the whole shell and much larger than that in area III and IV, and the maximum displacement of the whole shell locates at stagnation point ($C_{P,\,sta}$) in the middle height. In other words, the deformation in area I and II dominates the deformation and displacement of the whole shell due to the combination of push and suction there, which is also similar to the rings under $O_{rth}(\theta)$.

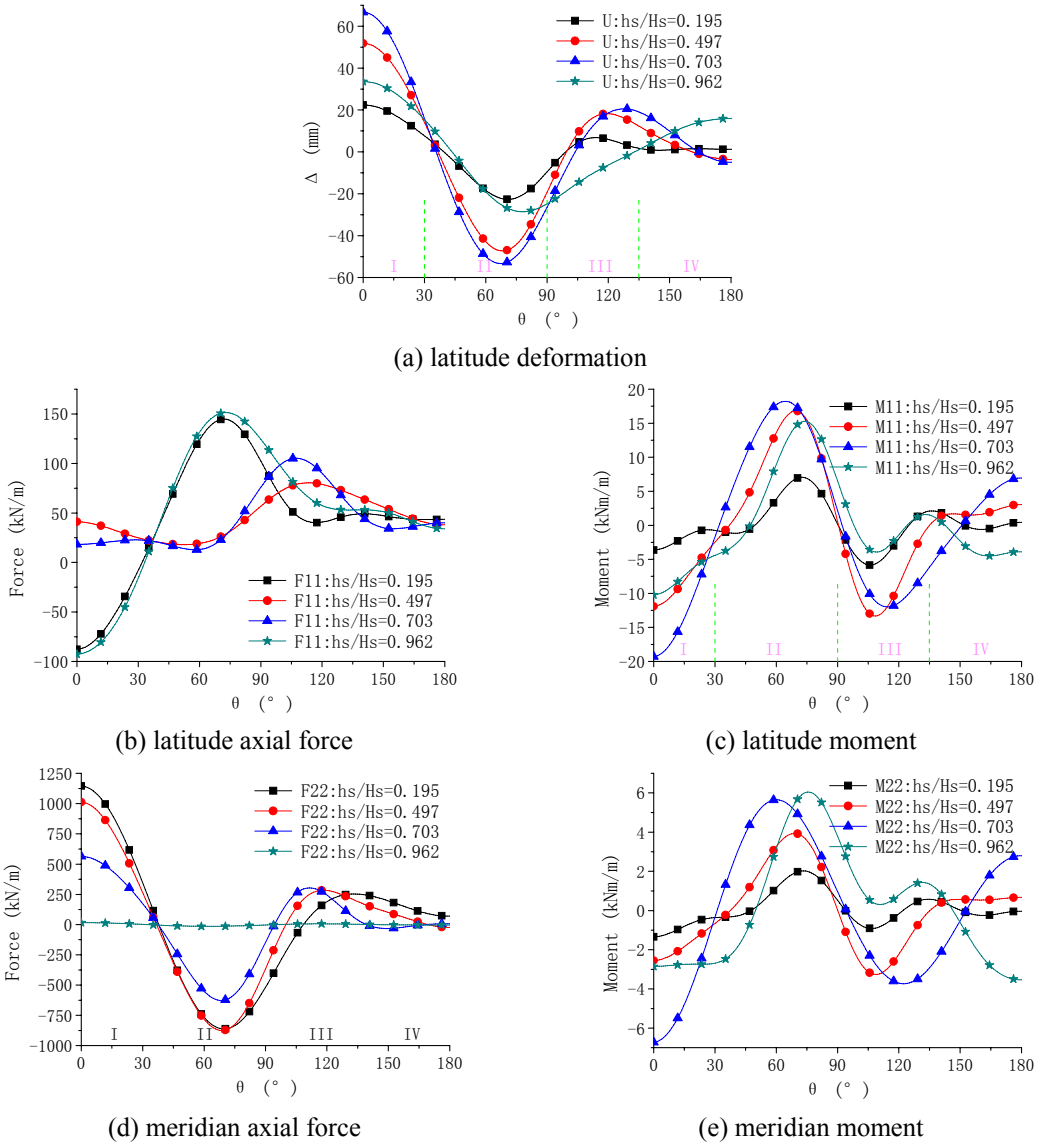

(a) latitude deformation

(b) latitude axial force

(c) latitude moment

(d) meridian axial force

(e) meridian moment

Fig. 6 Latitude distribution of wind load effects (TSPL Tower)

However, it should be noted that the deformation in area III is inward although the wind

pressure here is outward suction. That's because the huge convexity in area II and the extremely slight deformation in area IV induce the concavity in area III to meet the deformation compatibility condition (Fig. 6 (a)), and this forms a "triangle" deformation in the bottom and middle shell. In the top shell, it's far away from foundation and it's free at top edge, so there is less restriction for latitude deformation. Therefore, area III and IV show greater trend to go inward in the top shell for deformation compatibility just like the rings under $O_{\text{rth}}(\theta)$, and an "ellipse" deformation is formed.

Distributions of internal forces under wind loads are determined by the deformation pattern above. For latitude moment M_{11}, the outward (area II) and inward (area I, III) deformation gives contrary curvature compared with the original circle. Therefore, M_{11} is positive for outward and negative for inward separately ($M_{11\text{O}}$, $M_{11\text{I}}$, O/I: Outward/Inward). The maximum M_{11}, $M_{11\text{O, M}}$, locates around the minimum point of $C_{\text{P}}(\theta)$ ($C_{\text{P, min}}$) where the most outstanding outward curvature appears. Area I and III are occupied by $M_{11\text{I}}$ which both have significant inward curvature. These are all similar to the moment distribution of the rings under $O_{\text{rth}}(\theta)$. As the curvature in area III changes with the height, the location of minimum M_{11}, $M_{11\text{I, M}}$, will change with the height correspondingly (Figs. 6(c) and 7(b)): i.e., the location of $M_{11\text{I, M}}$ is around $C_{\text{P, sta}}$ in the top half shell but $C_{\text{P, sep}}$ in the bottom half. This is also the reflection of latitude deformation: "ellipse" deformation at the top shell relieves the curvature in area III; for "triangle" deformation at the bottom half, however, curvature in area III is somewhat severer than that in area I, which results in slight higher amplitude of latitude moment, $M_{11\text{A}}$ (A: Amplitude), around $C_{\text{P, sep}}$ than the $M_{11\text{A}}$ around $C_{\text{P, sta}}$. Furthermore, horizontal latitude deformation alters the shell's original meridian curve, and meridian curvature at the three locations ($C_{\text{P, sta}}$, $C_{\text{P, min}}$ and $C_{\text{P, sep}}$) is the most outstanding as well, so the maximum amplitude of meridian moment $M_{22\text{A, M}}$ locates there likewise.

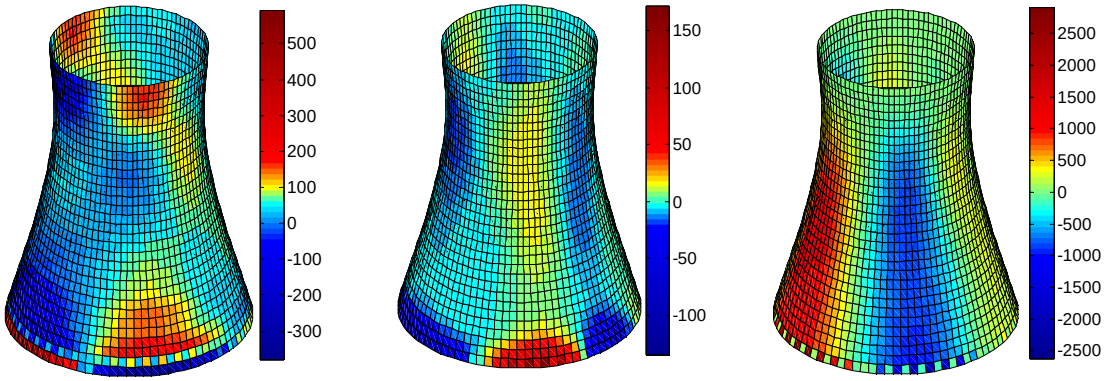

(a) latitude axial force (kN/m) (b) latitude moment (kNm/m) (c) meridian axial force (kN/m)

Fig. 7 Surface distribution of wind load effects (TSPL Tower)

For latitude axial force F_{11} (Fig. 6(b)), the maximum amplitudes of tension and compression ($F_{11\text{T, M}}$, $F_{11\text{C, M}}$; T/C: Tension/Compression; M: Max for T and Min for C) locate around $C_{\text{P, sta}}$ in the bottom shell and $C_{\text{P, min}}$ in the top shell respectively, because the deformation there is minor owing to the strong stiffness provided by the foundation and stiffening ring at top edge. This is

also similar to the rings under $O_{rth}(\theta)$. In the middle shell, however, the deformation there is dramatic due to the weak stiffness and the whole latitude is occupied by tension. The location of maximum tension $F_{11T,\,M}$ transfers to $C_{P,\,sep}$ for the deformation compatibility (Fig. 6(a)). For structure design, F_{11} in the top shell should be noted, the "ellipse" deformation induces larger maximum amplitude of latitude axial force $F_{11A,\,M}$ there than the one induced by "triangle" in the middle shell, but the thickness in middle and top shell are almost the same.

Meridian axial force F_{22} in area I and III is tension because the deformation there is inward, which is consistent with the original negative meridian curve (Fig. 6(d)). On the contrary, the outward deformation in area II produces compression. Dominated by the latitude deformation, the latitude distribution of F_{22} is similar to the latitude deformation, and the maximum amplitudes of meridian tension and compression, $F_{22T,\,M}$, $F_{22C,\,M}$, locate around $C_{P,\,sta}$ and $C_{P,\,min}$ respectively (Figs. 6 (d) and 7(c)). It's noteworthy that F_{22} aggregates downward along the height steadily, and this is the unique character of F_{22}.

As stated previously, a HCT under wind loads can be regarded as a structure coupled by rings and cantilever beams. Because of the overall along-wind action which expressed by C_D, there is along-wind overturning moment for a HCT and the moment aggregates downward if the HCT is regarded as a cantilever beam. Nevertheless, the resisting moment is mainly reserved as meridian axial force along the latitude for HCTs rather than explicit section resisting moment just as cantilever beams (Fig. 8(a)). Because the latitude distribution of F_{22} is almost the same for the whole height, the F_{22} will aggregate downward to provide resisting overturning moment. Moreover, the aggregation is amplified in the top shell but weakened in the bottom by the radius variation along the height, because it serves as the moment arm for meridian axial force: the radius decreases in the top shell but increases in the bottom shell along the height downward. The resisting overturning moments provided by F_{22} and M_{22} are illustrated in Fig. 8(b). It's clearly that the resisting overturning moment in each cross section is almost fully provided by F_{22} but M_{22} is just a local effect.

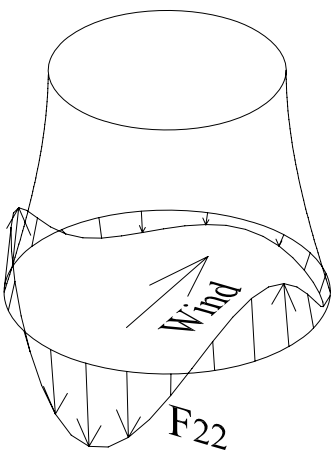

(a) latitude distribution of F_{22}

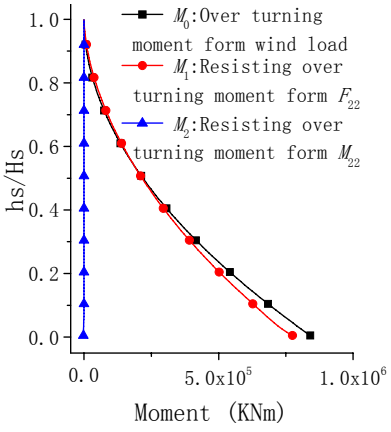

(b) resisting overturning moments provided by F_{22} and M_{22}

Fig. 8 Resisting overturning moment from meridian axial force F_{22} (TSPL Tower)

For HCTs, the structure design in latitude and meridian directions are independent and there is controlling internal force in the two directions respectively. From Figs. 6 and 7, it can be found that the structure design under wind loads is controlled by F_{22} and M_{11} completely for the whole shell; the latitude axial force F_{11} in the top shell can't be ignored as well. M_{22} in the whole shell and F_{11} in the middle and bottom shell have hardly influence on structure design compared with F_{22} and M_{11}. So the reasonable indicators for the relationship between wind pressure distribution and responses would be F_{22} and M_{11}. Of course, the two indicators should be studied separately because their sensitivities to the variation of $C_P(\theta)$ are different.

From the latitude distribution comparison among $C_P(\theta)$ (Fig. 1), deformation (Fig. 6(a)) , meridian axial force F_{22} (Fig. 6(b)) and latitude moment M_{11} (Fig. 6(c)), it can be deduced that their latitude distributions are similar, especially in windward and sideward regions; the maximum deformation and the maximum amplitudes of internal forces all occur around the point of $C_{P, sta}$, $C_{P, sep}$ and $C_{P, min}$ which all are the peak values of $C_P(\theta)$. In other words, latitude distribution of $C_P(\theta)$ determines the latitude distribution of load effects. Additionally, the latitude distributions of deformation and latitude moment M_{11} are both similar to that of rings, the latitude distribution of meridian axial force F_{22} also is the reflection of latitude deformation, and its aggregation downward is the reflection of mechanical performance of cantilever beams. Consequently, HCTs can be regarded as the coupling of horizontal rings and meridian cantilever beams form the analysis of mechanical performance under wind loads.

Table 2 Wind pressure distribution adjustments

Categories	Adjustment regions and methods	Resistance/Drag coefficient C_D
Leeward:	$105\leq\theta\leq180$ $C_{P, LWi}(\theta)=C_P(\theta)+0.2\times(3-i)$;	-0.011, 0.187, (0.385), 0.583, 0.781
LWi (i=1~5)	$90\leq\theta\leq105$ $C_{P, LWi}(\theta)=C_P(\theta)+0.2\times(3-i)\times(\theta-90)/(105-90)$	
Sideward:	$C_{P, SWi}(\theta)=C_P(\theta)+0.2\times(3-i)\times((C_P(\theta)+0.55)/(C_{P, min}+0.55))^2$	0.440, 0.412, (0.385), 0.358, 0.330
SWi (i=1~5)	$C_P(\theta)\leq-0.55$	
Windward:	$C_{P, SWi}(\theta)=C_P(\theta)+0.25\times(2-i)\times((C_P(\theta)+0.25)/(C_{P, sep}+0.25))^2$	0.462, (0.385), 0.308, 0.231, 0.153, 0.076
WWi (i=1~6)	$C_P(\theta)\geq-0.25$	
Location of $C_{P, min}$: LOCi (i=1~6)	i=1~6, LOC=90.0°, 84.2°, 78.4°, (72.6°), 66.3°, 60.0°	0.730, 0.606, 0.488, (0.385), 0.286, 0.201

Note: The origin distribution is form Chinese code, namely 'Norm', which is LW3, SW3, WW2 and LOC4 for different categories

3. Influence of different $C_P(\theta)$ on wind load effects

According to the perception on the mechanical performance of HCTs under wind loads, the influence of $C_P(\theta)$ on the wind load effects will be discussed in the following. $C_P(\theta)$ from Chinese code (DL/T 5339-2006) is adjusted artificially, including the wind pressure amplitude in windward, sideward and leeward and also the location of $C_{P, min}$ respectively (Table 2, Fig. 9), and wind load

effects are analyzed for different adjustments. In the adjustments of wind pressure amplitude of the three regions, the pressure in neighboring areas is adjusted continuously and gradually to maintain the original wind pressure distribution pattern. What should be noted is that the wind pressure adjustments target at the peak value in windward, so a new peak value is brought out around θ=30° in the steady decrease of windward push (Fig. 9). The adjustment of the location of $C_{P,\,min}$ is achieved through contraction and amplification of latitude angle θ.

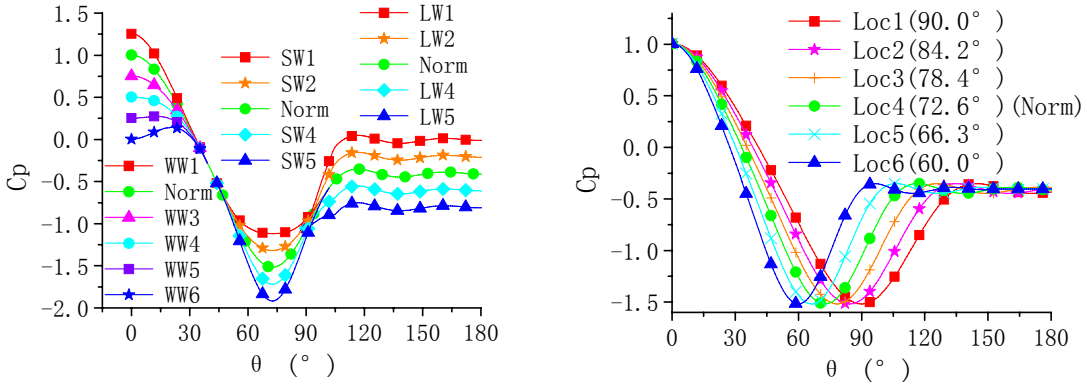

(a) different wind pressure amplitudes of the three regions

(b) different locations of $C_{P,\,min}$

Fig. 9 Adjustments of the wind pressure distribution $C_P(\theta)$

3.1 Wind pressure distribution in leeward, $C_{P,\,LW}$

Latitude deformation for different $C_{P,\,LW}$ is shown in Fig. 10(a). The deformation tends to be alleviated with the increase of suction in leeward. The most remarkable influence is on area III where the leeward suction acts directly; and the amplitudes of M_{11} and F_{22} in area III decrease greatly with the deformation there but show less change in other areas (Fig. 10(b)). As stated previously, the deformation under wind pressure is dominated by windward and sideward; wind pressure in the single windward and two sideward is analogous with $O_{rth}(\theta)$ but with the push missed in leeward (Fig. 3). Apparently, the deformation will be deteriorated if the wind pressure in leeward is push but smoothed if suction. Or in another way, for the wind pressure distribution $C_P(\theta)$ which shares certain similarity with $O_{rth}(\theta)$ in Fig. 3, the greater gap between tension and compression of the two axes, the sharper deformation. Consequently, the deformation is alleviated with the increase of leeward suction. In addition, the deformation in area I is smoothed with the increase of leeward suction, yet the influence on area I is much less than that on area III and II; that means wind loads have obvious local effects on the load effects: variation of leeward suction has major influence on area III but minor on area I. Therefore, the value of the maximum displacement descends slightly with the increase of leeward suction but its location is hardly influenced by the leeward suction variation (Fig. 10(a)).

Alleviation in deformation owing to the increase of leeward suction results in descent of the amplitudes of $M_{11O,\,M}$, $M_{11I,\,M}$ and $F_{22C,\,M}$ in the whole shell apart from $F_{22T,\,M}$ which shows no sensitivity to the variation of leeward suction (Figs. 11(b) and (c)). This is definite according to the

relationship between deformation and internal forces. Because $F_{22T,M}$ and $F_{22C,M}$ always locate around $C_{P,sta}$ in area I and $C_{P,min}$ in area II respectively for different $C_{P,LW}$, the sensitivity of $F_{22T,M}$ to the variation of $C_{P,LW}$ is much less than that of $F_{22C,M}$ for the local effects of wind loads, just as the deformation in area I and area II. From the point of overturning moment, the amplitudes of F_{22C} in area II and F_{22T} in area III both should descend so as to balance the increased overturning moment results from the increase of leeward suction (Fig. 10(b)). $M_{11O,M}$ in the whole shell locates around $C_{P,min}$ for different $C_{P,LW}$ and therefore its sensitivity to the variation of $C_{P,LW}$ is nearly uniform in the whole shell. $M_{11I,M}$ locates around $C_{P,sta}$ in area I for the top half shell and around $C_{P,sep}$ in area III for the bottom half shell respectively. The sensitivity of M_{11I} to the variation of $C_{P,LW}$ is different for area I and III just as the deformation in the two areas, and therefore the amplitude of $M_{11I,M}$ in the top half shell descends slowly with the increase of leeward suction but quickly in the bottom half (Fig. 11(c)). $M_{22A,M}$ has similar performance to $M_{11A,M}$ which are both issued from the latitude deformation (Fig. 11(d)).

For latitude axial force F_{11} in the top and bottom shell, $F_{11C,M}$ and $F_{11T,M}$ locate around $C_{P,sta}$ and $C_{P,min}$ respectively, and their locations and amplitudes are both independent on the variation of $C_{P,LW}$ due to its little influence there. In the middle shell, F_{11} is tension for the whole latitude and $F_{11T,M}$ locates around $C_{P,sep}$. Although $F_{11T,M}$ there ascends with the increase of leeward suction, still it is much less than $F_{22T,M}$, even less than the design value of concrete tension strength, and therefore has no practical sense for structure design (Fig. 11(a)). Consequently, it can be deduced that the controlling indicators of structure design under wind loads generally descend with the increase of leeward suction such as $M_{11A,M}$, $F_{22C,M}$ and deformation, or remain the same, such as $F_{22T,M}$ and the $F_{11A,M}$ in top shell. However, the leeward suction, -0.45 from experimental results, was "conservatively" defined to be -0.5 (Harnach and Niemann 1980) and accepted by Germany code. It's clear that this alteration would be a little dangerous according to the analysis above.

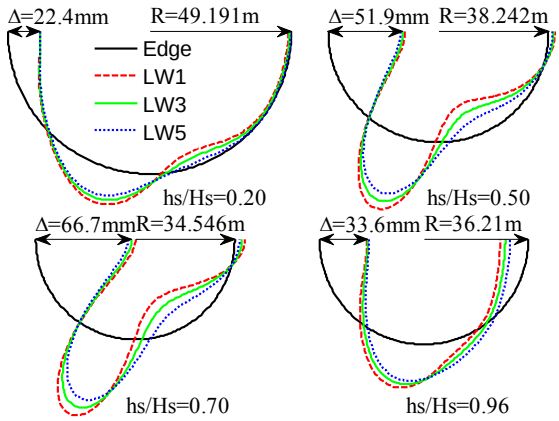

(a) latitude deformation in different heights

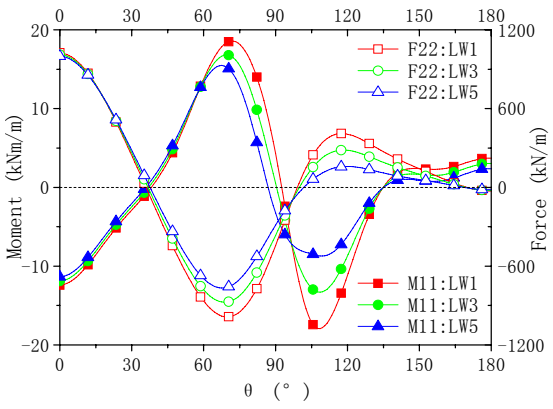

(b) latitude distribution of F_{22} and M_{11} at hs/Hs=0.50

Fig. 10 Wind induced responses for different $C_{P,LW}$ (TSPL Tower)

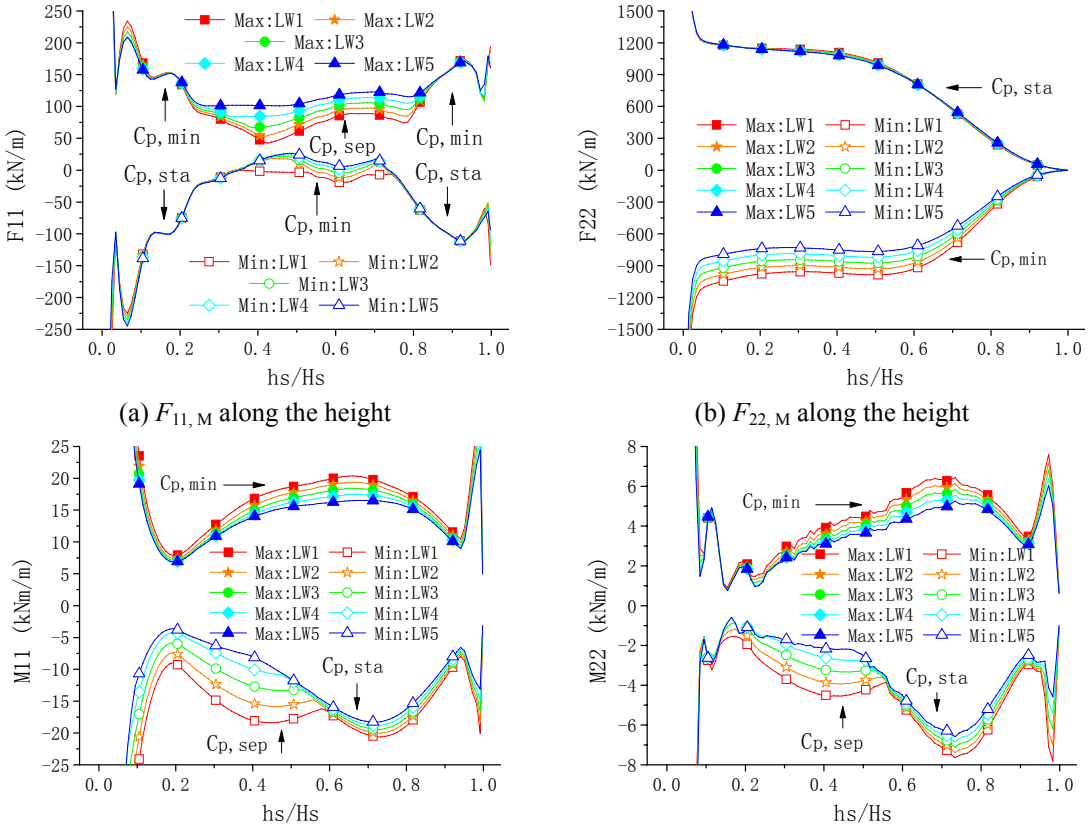

(a) $F_{11,\,M}$ along the height

(b) $F_{22,\,M}$ along the height

(c) $M_{11,\,M}$ along the height

(d) $M_{22,\,M}$ along the height

Fig. 11 Maximum internal forces along the height for different $C_{P,\,LW}$ (TSPL Tower)

3.2 Wind pressure distribution in sideward, $C_{P,\,SW}$

Latitude deformation for different $C_{P,\,SW}$ is shown in Fig. 12(a). Contrary to the influence of the increase of leeward suction, the deformation tends to be aggravated with the increase of sideward suction. The most remarkable influence is on area II where the sideward suction acts directly; and the amplitudes of M_{11} and F_{22} in area II increase greatly with the deformation there but show less change in other areas (Fig. 12(b)). As stated previously, the sideward suction is analogous to the uniaxial tension in Fig. 3 and its increase will aggravate the latitude deformation. The deformation in area I, II and III are all influenced greatly by the variation of sideward suction which is one of the controlling factors for latitude deformation, yet the influence on area I and III are obviously less than that on area II: what indicates the local effects of wind loads as well. In addition, the value of the maximum displacement ascends with the increase of sideward suction but its location is always the same for all $C_{P,\,SW}$ (Fig. 12(a)).

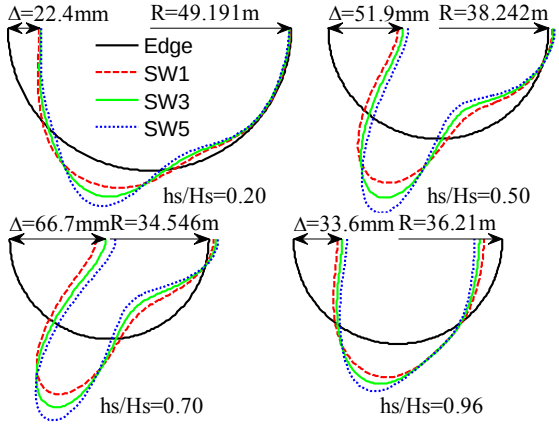

(a) latitude deformation in different heights

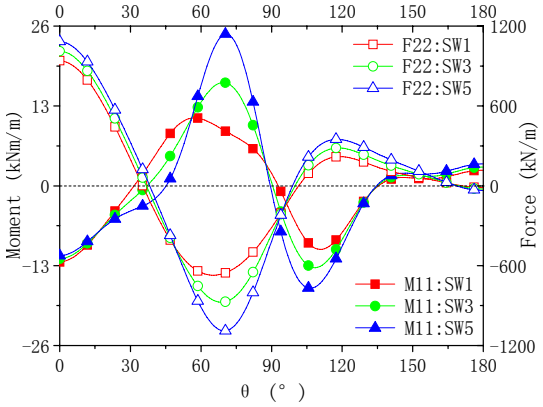

(b) latitude distribution of F_{22} and M_{11} at hs/Hs=0.50

Fig. 12 Wind induced responses for different $C_{P,SW}$ (TSPL Tower)

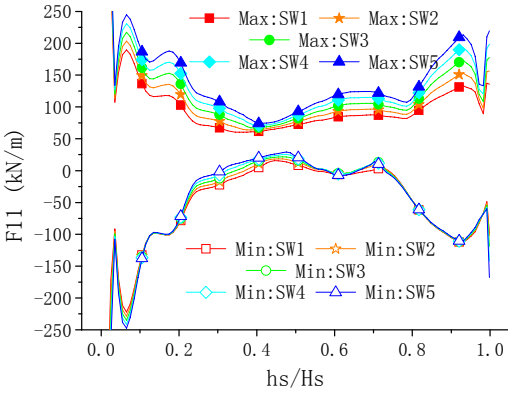

(a) $F_{11,M}$ along the height

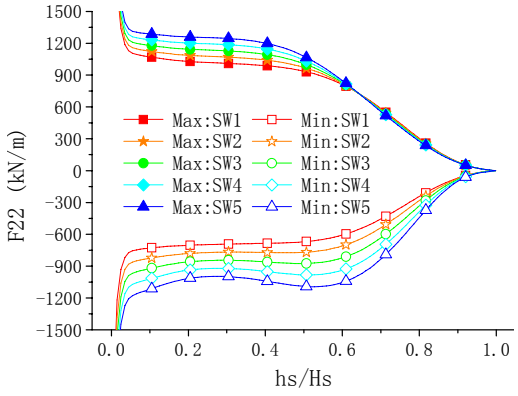

(b) $F_{22,M}$ along the height

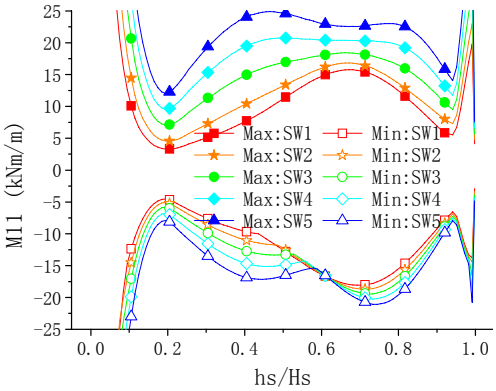

(c) $M_{11,M}$ along the height

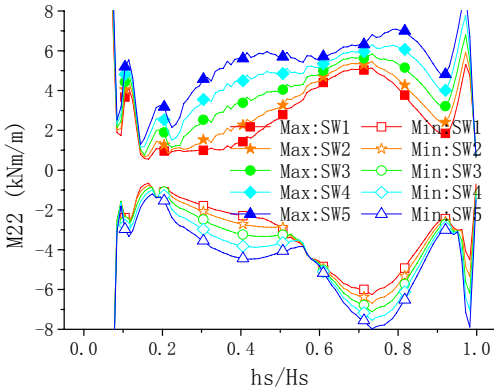

(d) $M_{22,M}$ along the height

Fig. 13 Maximum internal forces along the height for different $C_{P,SW}$ (TSPL Tower)

Aggravation in deformation owing to the increase of sideward suction results in ascent of the amplitudes of $M_{11O,M}$, $M_{11I,M}$, $F_{22T,M}$ and $F_{22C,M}$ in the whole shell because their locations are all in the influence areas of sideward suction (Figs. 13(b) and (c)). The locations of $F_{22C,M}$, $F_{22T,M}$ and $M_{11O,M}$ are independent of the variation of $C_{P,SW}$, and therefore their sensitivities to the variation of $C_{P,SW}$ are nearly uniform in the whole shell. The inward deformation in area III and I are both aggravated, but the former has greater influence on the curvature which results in greater amplitude of M_{11I} than that in area I, because area I has much wider scope than area III for its bilateral symmetry. $M_{11I,M}$ locates around $C_{P,sta}$ in area I for the top half shell and around $C_{P,sep}$ in area III for the bottom half shell respectively, and therefore the sensitivity of $M_{11I,M}$ to the variation of $C_{P,SW}$ in the whole shell is less than $M_{11O,M}$ which locates in area II acted by $C_{P,SW}$ directly. $M_{22A,M}$ has similar performance to $M_{11A,M}$ which are both issued from the latitude deformation (Fig. 13(d)).

For latitude axial force $F_{11C,M}$ in the top and bottom shell which locates around $C_{P,sta}$, its location and amplitude are both independent on the variation of $C_{P,SW}$ due to its little influence on area I in the top and bottom shell. $F_{11T,M}$ in the whole shell ascends with the increase of sideward suction because it locates around $C_{P,min}$ or $C_{P,sep}$ where the deformation are both intensified.

However, $F_{11A,M}$ still is much less than $F_{22A,M}$ and has no practical sense for structure design except in the top shell (Fig. 13(a)). Consequently, it can be deduced that the controlling indicators of structure design under wind loads generally ascend with the increase of sideward suction such as $M_{11A,M}$, $F_{22A,M}$, the $F_{11T,M}$ in top shell and deformation.

3.3 Wind pressure distribution in windward, $C_{P,WW}$

Latitude deformation for different $C_{P,WW}$ is shown in Fig. 14(a). Same to the influence of the increase of sideward suction, the deformation tends to be aggravated with the increase of windward push, and the influence is mainly on area I in the whole shell and also on area II in the middle shell because there is no corresponding push in leeward to produce uniaxial compression. As a result, the amplitudes of F_{22} and M_{11} in area I ascend remarkably with the increase of $C_{P,WW}$, but almost remain the same in other areas (Fig. 14(b)). All of them indicate the local effects of wind loads as well. In addition, the value of the maximum displacement ascends with the increase of $C_{P,WW}$ and the location is always in area I but transfers to area II only for $C_{P,WW6}$.

Aggravation in deformation owing to the increase of windward push results in great ascent of the amplitude of $M_{11O,M}$ in the top half shell but slight descent in the bottom half which locates around $C_{P,min}$ for all $C_{P,WW}$. Also, the amplitude of $M_{11I,M}$ in the whole shell ascends with the windward push. However, $M_{11I,M}$ in the top half shell show greater sensitivity because of the different location of $M_{11I,M}$ in the top and bottom half shell, as well as the local effects of wind loads (Fig. 15(c)). $M_{22A,M}$ has similar performance to $M_{11A,M}$ which are both issued from the latitude deformation (Fig. 15(d)).

$F_{22T,M}$ and $F_{22C,M}$ locate around $C_{P,sta}$ and $C_{P,min}$ respectively for all $C_{P,WW}$ except that $F_{22T,M}$ transfers to the new peak value of windward pressure for $C_{P,WW6}$, so the amplitudes of $F_{22T,M}$ and $F_{22C,M}$ both ascend in the whole shell with the increase of windward push which aggravates the deformation in area I and II (Fig. 15 (b)). Of course the amplitude ascent of $F_{22T,M}$ is rapider than that of $F_{22C,M}$ on account of the greater deformation aggravation, and their ascents can also be explained by the effect of overturning moment which ascends with the increase of windward push.

For latitude axial force F_{11} (Fig. 15(a)), $F_{11T,M}$ locates around $C_{P,min}$ or $C_{P,sep}$ and its location and amplitude are not sensitive to the variation of $C_{P,WW}$; on the other hand, the amplitude of $F_{11C,}$

$_{M}$ ascends with the increase of windward push. Consequently, it can be deduced that the controlling indicators of structure design under wind loads generally ascend with the increase of windward push such as $M_{11A,M}$, $F_{22A,M}$ and deformation, or remain unchanged, such as the $F_{11A,M}$ in top shell.

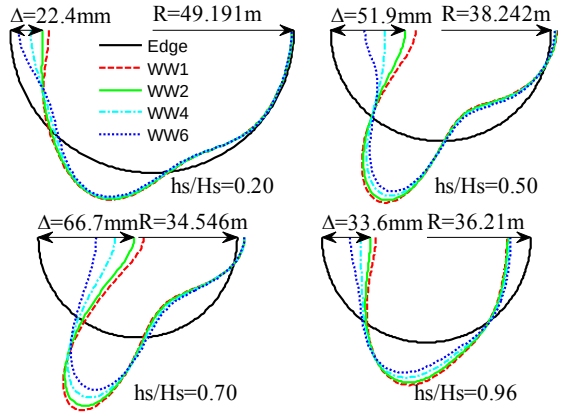

(a) latitude deformation in different heights

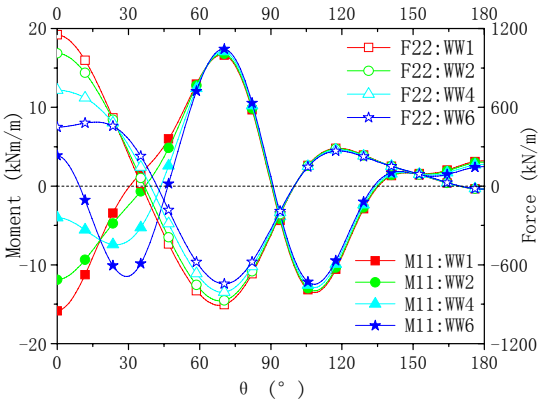

(b) latitude distribution of F_{22} and M_{11} at hs/Hs=0.50

Fig. 14 Wind induced responses for different $C_{P,WW}$ (TSPL Tower)

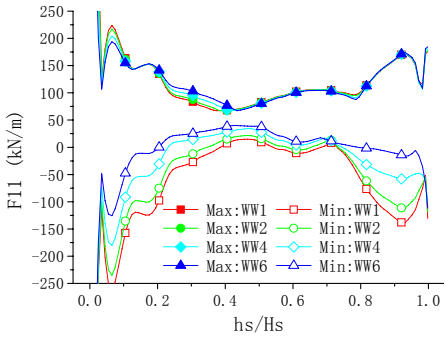

(a) $F_{11,M}$ along the height

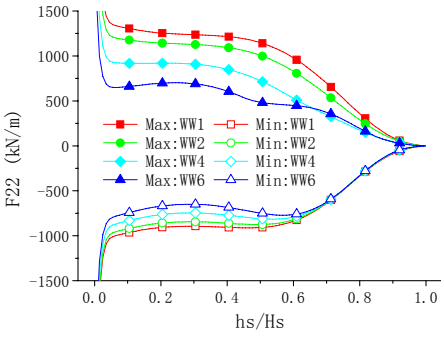

(b) $F_{22,M}$ along the height

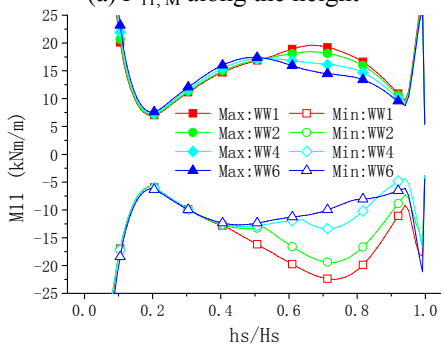

(a) $M_{11,M}$ along the height

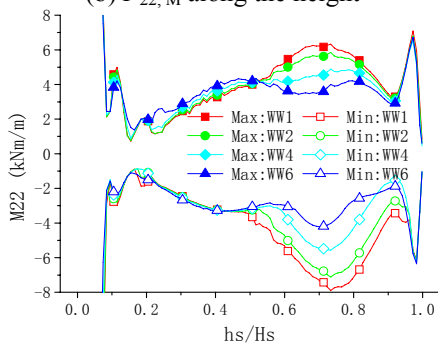

(b) $M_{22,M}$ along the height

Fig. 15 Maximum internal forces along the height for different $C_{P,WW}$ (TSPL Tower)

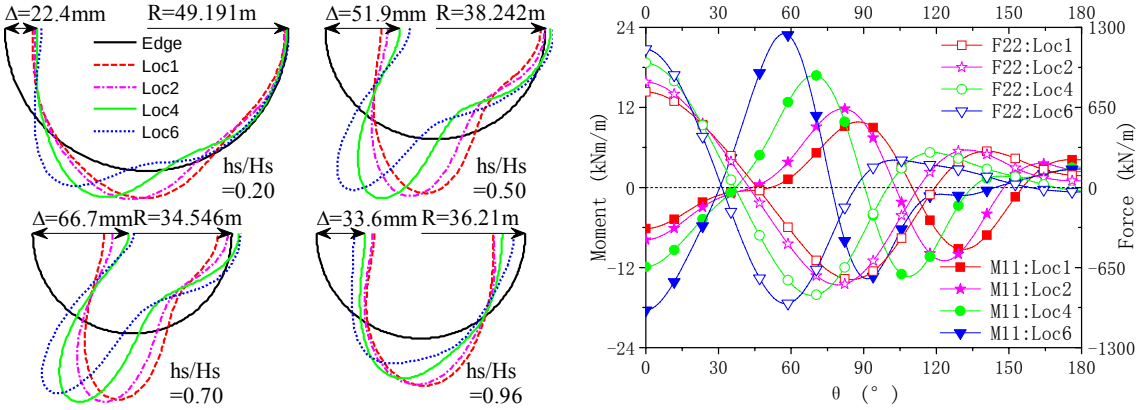

(a) latitude deformation in different heights

(b) latitude distribution of F_{22} and M_{11} at hs/Hs=0.50

Fig. 16 Wind induced responses for different $C_{P,\,LOC}$ (TSPL Tower)

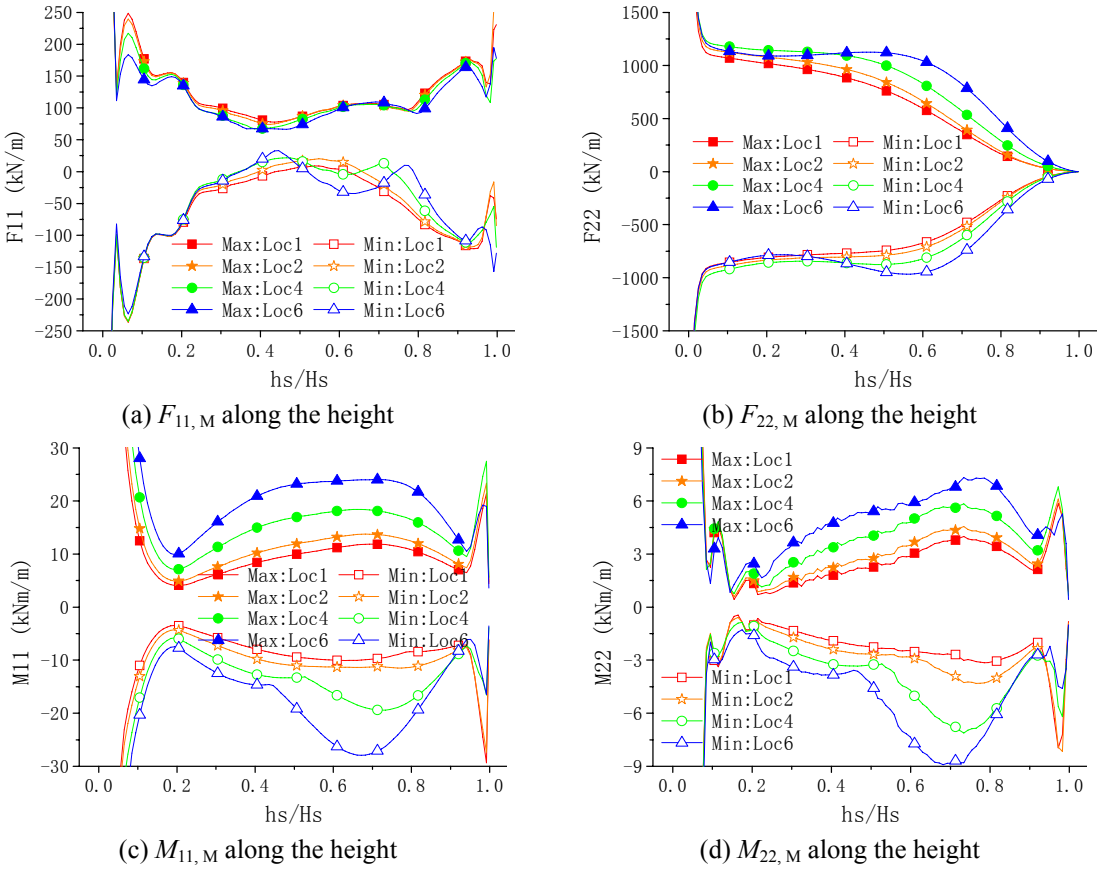

(a) $F_{11,\,M}$ along the height

(b) $F_{22,\,M}$ along the height

(c) $M_{11,\,M}$ along the height

(d) $M_{22,\,M}$ along the height

Fig. 17 Maximum internal forces along the height for different $C_{P,\,LOC}$ (TSPL Tower)

3.4 Location of $C_{P,\,min}$

Latitude deformation and internal forces for different location of $C_{P,\,min}$ are shown in Figs. 16 and 17. As stated in Section 2.2, the deformation in the bottom and middle shell is similar with the C_P distribution and like a triangle. With the location of $C_{P,\,min}$ moving ahead, the C_P distribution is much like a triangle, so latitude deformation aggravates and all internal forces ascend for the whole shell except the top and bottom edge. Another, the latitude deformation pattern and the latitude distributions of internal forces are always in accordance with the C_P distribution, which also confirms the conclusion in section 2.2 that the latitude distributions of load effects are determined by the latitude distribution of $C_P(\theta)$. Moreover, the deformation and internal forces in area I and II, where the sideward suction acts directly, are much influenced because of the local effects of load effects. Consequently, it can be deduced that the controlling indicators of structure design under wind loads generally ascend with the location of $C_{P,\,min}$ moving ahead such as $M_{11A,\,M}$, $F_{22A,\,M}$ and deformation.

4. Analysis of influence for different $C_P(\theta)$

Latitude wind pressure shows remarkable local effects on load effects. Wind pressure in one area mainly influences the load effects in this area and in the neighboring areas, and the influence dissipates with distance, for example $C_{P,\,LW}$ on area III, IV; $C_{P,\,SW}$ on area II, I, III; and $C_{P,WW}$ on area I and on area II in the middle shell. Moreover, it can be perceived that wind load effects in the shell dependent directly on latitude wind pressure distribution $C_P(\theta)$, i.e., the non-uniformity of $C_P(\theta)$ (Table 3). Because $C_P(\theta)$ has just one crest around $C_{P,\,sta}$, two hollows around $C_{P,\,min}$, and nearly unifrom $C_{P,\,LW}$; increase of windward push and sideward suction as well as decrease of leeward suction results in more nonuniform $C_P(\theta)$ and more aggravated controlling wind load effects in structure design. Also, when the location of $C_{P,\,min}$ moves ahead, the $C_P(\theta)$ distribution become more nonuniform as well because the distance between the crest and hollow is shorten, and therefore the wind load effects become more aggravated. When the $C_P(\theta)$ tends to uniformity, the deformation and characteristic internal forces are all smoothed and their maximum amplitudes all decrease. Actually, this is what the mechanical performance of rings under circular pressure.

Therefore, it is conservative to choose the higher sideward suction and lower leeward suction in structure design when $C_P(\theta)$ is not clear for sideward and leeward.

It can be seen in Figs. 11, 13 and 15 that the most sensitive internal force to $C_P(\theta)$ is $F_{11T,\,M}$ in the middle shell due to its small value, but F_{11} is tension for the whole latitude in the middle shell which will be neutralized by the compression induced by self weight to some extent and therefore won't be the controlling force for structure design. The dependence of $M_{11A,\,M}$ and $M_{22A,\,M}$ on the variation of $C_P(\theta)$ are almost the same, but both the sensitivity of $M_{11A,\,M}$ to the variation of $C_P(\theta)$ and the amplitude of $M_{11A,\,M}$ are much outstanding than those of $M_{22A,\,M}$. For these reasons, $F_{22T,\,M}$ and $M_{11A,\,M}$, which are also controlling forces for structure design, will be reasonable indicators for the evaluation of influence on wind load effects from the variation of $C_P(\theta)$. What should be noted is that the roles of M_{11A} and F_{22T} from wind loads in structure design are not identical. M_{11A} from wind loads will be added by the thermal effects but F_{22T} from wind loads will be neutralized to some extents by the gravity effects. So the structure design will be much influenced by the variation of F_{22T} but not the M_{11A} from wind loads. Also, if proper minimum circumferential reinforcement is specified, such as the British standard 4485, the variation of M_{11A} from wind

loads will have no practical influence on structure design, although it is more sensitive than F_{22A} to the variation of $C_P(\theta)$. In addition, it can be seen in Figs. 11, 13 and 15 that the influence on $F_{22A,\,M}$ is almost the same for the whole shell, but the influence on $M_{11A,\,M}$ is quite different in top and bottom shell. Consequently, the $F_{22T,\,M}$ is the more reasonable indicator than $M_{11A,\,M}$. The meridian tension stress is always used for interference effects research as well (Armitt 1980, Niemann and Köpper 1998, Orlando 2001) and it is the represent of F_{22T} actually. Table 3 gives the critical internal forces and their locations which are influenced greatest by $C_P(\theta)$.

Another one should be sated is the reference position (or the reference height) of $F_{22T,\,M}$. Ideally, this reference position should be the same for different adjustment of $C_P(\theta)$, and $F_{22T,\,M}$ at the selected position should show the most remarkable sensitivity along the height to the variation of $C_P(\theta)$. However, the most dangerous point for meridian net tension located in area of hs/Hs=0.3~0.6 around $C_{P,\,sta}$ in structure design (Noh 2005), but the sensitivity of $F_{22T,\,M}$ to the variation of $C_P(\theta)$ is not uniform even just in this height scope, especially for the variation of location of $C_{P,\,min}$. Ultimately, the reference position is selected for each adjustment respectively for convenience (Table 3), and at the selected position, $F_{22T,\,M}$ shows remarkable but not the most remarkable sensitivity to the variation of $C_P(\theta)$.

For consistent comparison, the influence on wind-induced responses (Response Influence Factor, *RIF*) and fitting expressions are given in Fig. 18 for leeward, sideward and windward amplitude and the location of $C_{P,\,min}$ respectively. The relationship between $F_{22T,\,M}$ and each influence factor is nearly linear, and can be expressed universally by

$$RIF_i = 1.0 + a_i(x_i - 1.0) + b_i(x_i - 1.0)^2; \qquad \begin{aligned} x_1 &= C_{P,MeanLee} / -0.39 \\ x_2 &= C_{P,Min} / -1.5186 \\ x_3 &= C_{P,Max} / 1.0 \\ x_4 &= Loc / 72.6 \end{aligned} \tag{2}$$

in which $C_{P,\,Max}$, $C_{P,\,Min}$, $C_{P,\,MeanLee}$ are the maximum coefficient, the minimum coefficient and the mean coefficient in leeward of $C_P(\theta)$; *Loc* is latitude location of the minimum coefficient; constant coefficients, a_i and b_i, are the influence weight factors of x_i and coefficient b is only used for x_4. From the amplitude of a_i, it's obvious that the variation of location of $C_{P,\,min}$ has the most prominent influence on $F_{22T,\,M}$, the amplitudes of windward and sideward follow behind, and the amplitude in leeward apply nearly no influence. This is also the reflection of the local effects of load effects because $F_{22T,\,M}$ always locates around $C_{P,\,sta}$.

To verify the universality of the relationship between $F_{22T,\,M}$ and the distribution of $C_P(\theta)$ for other HCTs, another three HCTs are analyzed and their constant coefficients are listed in Table 4. The constant coefficients for different HCTs show little difference, so their mean values can be used in practical application. On the foundation of the independent *RIF* expressed by Eq. (2) and the mean values of constant coefficients, a comprehensive *RIF* (Eq. (3)) including all the four parameters is obtained based on the following two hypotheses: the first, the influence from x_1 to x_3 can be added together, the total influence from x_1 to x_3 and the influence from x_4 should be multiplied; and the second, the different reference locations among the four parameters can be ignored.

$$RIF = (0.19 - 0.244C_{\mathrm{P,Min}} + 0.439C_{\mathrm{P,Max}}) \times (3.102 - 2.85\frac{Loc}{72.6} + 0.747(\frac{Loc}{72.6})^2) \quad (3)$$

According to Eq. (3), the *RIF* will be less than 1.0 if the wind pressure tends to be uniform. However, the $F_{22\mathrm{T,\,M}}$ in certain location won't be influenced by the change of $C_{\mathrm{P}}(\theta)$ and therefore $RIF \geq 1.0$ should be satisfied in practical application.

What should be noted is that this *RIF* is acquired from $F_{22\mathrm{T,\,M}}$, but can be used for other responses as well except M_{11}. From Section 2 and Section 3, it can be found that other responses except M_{11} nearly have no influence in structure design in all the $C_{\mathrm{P}}(\theta)$ adjustment, although they would be much sensitive to the $C_{\mathrm{P}}(\theta)$ variation. For M_{11}, the corresponding *RIF* can be got as well, but the reasonable and convenient method is setting proper minimum circumferential reinforcement because its role in structure design is limited.

Table 3 Load effects comparison from different wind pressure distributions (TSPL Tower)

Latitude domain name	Altitude of local pressure	Overall non-uniformity	Resistance coefficient C_{D}	Wind load effects	The most sensitive response
Leeward: LW*i* (*i*=1~5)	Up	Down	Up	Down	$M_{11\mathrm{I,\,M}}$ around $C_{\mathrm{P,\,sep}}$ in bottom half $F_{22\mathrm{C,\,M}}$ around $C_{\mathrm{P,\,min}}$ in whole shell
Sideward: SW*i* (*i*=1~5)	Up	Up	Down	Up	$M_{11\mathrm{O,\,M}}$ around $C_{\mathrm{P,\,min}}$ in whole shell $F_{22\mathrm{C,\,M}}$ around $C_{\mathrm{P,\,min}}$ in whole shell $F_{11\mathrm{T,\,M}}$ around $C_{\mathrm{P,\,min}}$ in top part
Windward: WW*i* (*i*=1~6)	Down	Down	Down	Down	$M_{11\mathrm{I,\,M}}$ around $C_{\mathrm{P,\,sta}}$ in top half $F_{22\mathrm{T,\,M}}$ around $C_{\mathrm{P,\,sta}}$ in whole shell
Location of $C_{\mathrm{P,\,min}}$: LOC*i* (*i*=1~6)	----	Up	Down	Up	$M_{11\mathrm{A,\,M}}$ in whole shell $F_{22\mathrm{T,\,M}}$ around $C_{\mathrm{P,\,sta}}$ in top half

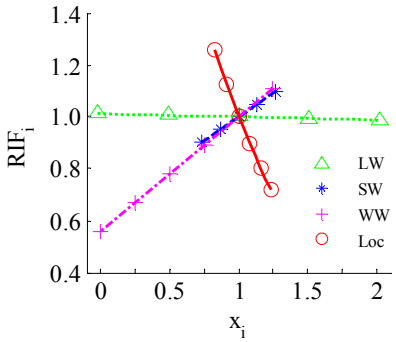

Fig. 18 Influence from different adjustment parameters (TSPL Tower)

Table 4 Constant coefficients of influence on $F_{22T,\,M}$ for different cooling towers

Constant coefficients	$C_{P,\,MeanLee}$	$C_{P,\,Min}$	$C_{P,\,Max}$	Loc	
	a_1	a_2	a_3	a_4	b_4
TSPL in India	-0.0122	0.3705	0.4393	-1.3548	0.7475
Pengcheng in China	-0.0122	0.3330	0.4650	-1.5381	1.1049
Ninghai in China	-0.0114	0.3233	0.4846	-1.4957	1.0595
Wuhu in China	-0.0088	0.3810	0.4384	-1.3325	0.6498
Mean value	-0.0111	0.3519	0.4568	-1.4302	0.8904
R.m.s./Mean value	-0.1430	0.0799	0.0486	-0.0713	0.2535

5. Conclusions

As high-rise and spatial thin-shelled structures, structure behavior analysis of HCTs is complicated by the three dimensional wind loads distribution. Although there are differences for $C_P(\theta)$ in different codes and $C_P(\theta)$ will be modified by interference effects, still some principles are deduced from above analysis. With some basic properties drawn from ring structures under circular pressure, the mechanical performance of HCT shell under wind loads was illustrated. Another, the influence of $C_P(\theta)$ on responses was studied by means of adjustment of $C_P(\theta)$ and *RIF* for different $C_P(\theta)$ was obtained consequently. The following summarizes the major findings and conclusions of this study:

1, As circular cross-section and thin-shelled structures, the mechanical performance of HCT shell under wind loads can be illustrated by the deformation of thin-walled ring structures, and this approach can contribute to the analysis of relationship between $C_P(\theta)$ and wind load effects. For example, the latitude deformations of both thin-walled rings and HCT shell are dominated by the non-uniformity of $C_P(\theta)$. Also, the latitude distribution of F_{22} is an implicit reflection of along-wind overturning moment for HCT shell and the shell's radius serves as the moment arm for F_{22}, so F_{22} aggregates downward along the height as the overturning moment.

2, Latitude wind pressure shows great local effects on internal forces and deformation. Wind pressure in one area mainly influences the load effects in this area and in the neighboring areas, and the influence dissipates with distance. The internal forces and deformation of HCT shell are primary dominated by wind pressure in sideward and windward which act as assistants for each other just as $O_{rth}(\theta)$.

3, Wind-induced responses of HCT shell are primarily influenced by the non-uniformity of $C_P(\theta)$ but not the local pressure amplitude C_P or overall resistance coefficient C_D. Latitude moment M_{11A} and meridian axial tension F_{22T} are always the controlling internal forces for different $C_P(\theta)$, but F_{22T} is more reasonable to be used for interference effects research. The sensitivity of F_{22T} to the wind pressure variation in different regions ranged as follows: the location of $C_{P,\,Min}$, the pressure amplitude in sideward, windward and leeward. Based on the sensitivity of $F_{22T,\,M}$ to different adjustment parameters of $C_P(\theta)$, a comprehensive response influence factor, *RIF*, is deduced to assess the F_{22T} for arbitrary $C_P(\theta)$. Moreover, this *RIF* can be used for other internal forces except M_{11}, because other responses except M_{11} have nearly no practical influence in structure design.

As stated at the beginning, this study is just confined to the static loads and responses, and only in this way the mechanism of influence of wind pressure distribution on wind-induced responses

can be obtained. Therefore, further study should be carried out with the dynamic effects included.

Acknowledgements

The authors would like to gratefully acknowledge the supports of the National Science Foundation of China (51021140005, 2009ZX06004-010-HYJY-21).

References

Abel, J.F., Billington, D.P., Nagy, D.A. and Wiita-Dworkin, C. (1982), "Buckling of cooling towers", *J. Struct. Div.*, **108**(10), 2162-2174.

ACI Standard, Manual of Concrete Practice, (1992), *Reinforced concrete tower shells: practice and commentary* (ACI 334.2R-91), American Concrete Institute, Detroit.

Andres, M. and Harte, R. (2006), "Buckling of concrete shells: a simplified numerical approach", *Int. J. Assoc. Shell Spatial Struct*., **47**(3).

Armitt, J. (1980), "Wind loading on cooling towers", *J. Struct. Div.*, **106**(3), 623-641.

British Standard (1996), *Code of practice for structural design and construction - Water Cooling Towers* (BS 4485 Part 4), British Standard Institution, London.

Cole, P.P., Abel, J.F. and Billington, D.P. (1975a), "Buckling of cooling-tower shells: state-of-the-art", *J. Struct. Div.*, **101**(6), 1185-1203.

Cole, P.P., Abel, J.F. and Billington, D.P. (1975b), "Buckling of cooling-tower shells: bifurcation results", *J. Struct. Div.*, **101**(6), 1205-1222.

Gopinath, S., Iyer, N., Rajasankar, J. and D'Souza, S. (2012), "Nonlinear analysis of RC shell structures using multilevel modelling techniques", *Eng. Comput.*, **29**(2), 104-124.

Harnach, R. and Niemann, H.J. (1980), "Influence of realistic mean wind loads on the static response and the design of high cooling towers", *Eng. Struct.*, **2**(1), 27-34.

John, A.D., Singla, G., Uphadyay, A. and Gairola, A. (2011), "Wind induced interference effect on rigid model of cooling tower", *Proceedings of the 13th International Conference on Wind Engineering*, Amsterdam, July.

Mang, H.A., Floegl, H., Trappel, F. and Walter, H. (1986), "Wind loaded reinforced-concrete cooling towers: buckling or ultimate load?", *J. Struct. Eng.*, **5**(3), 163-180.

Mungan, I. (1982), "Buckling of reinforced concrete cooling tower shells: BSS approach", *ACI Struct. J.*,**79**(5), 387-391.

NDRC (2006), *Code for hydraulic design of fossil fuel power plants*, DL/T 5339-2006, National Development and Reform Commission, Beijing. (in Chinese).

Niemann, H.J. (1980), "Wind effects on cooling-tower shells", *J. Struct.Div*., **106**(3), 643-661.

Niemann, H.J. and Köpper, H.D. (1998), "Influence of adjacent buildings on wind effects on cooling towers", *Eng. Struct.*, **20**(10), 874-880.

Noh, H.C. (2006), "Nonlinear behavior and ultimate load bearing capacity of reinforced concrete natural draught cooling tower shell", *Eng. Struct.*, **28**(3), 399-410.

Orlando, M. (2001), "Wind-induced interference effects on two adjacent cooling towers", *Eng. Struct.*, **23**(8), 979-992.

Sabouri-Ghomi, S., Kharrazi, M.H.K. and Javidan, P. (2006), "Effect of stiffening rings on buckling stability of R.C. hyperbolic cooling towers", *Thin Wall. Struct.*, **44**(2), 152-158.

Sun, T.F. and Zhou, L.M. (1983), "Wind pressure distribution around a ribless hyperbolic cooling tower", *Journal of Wind Engineering and Industrial Aerodynamics*, **14**(1-3), 181-192.

VGB-Guideline (2005), *Structural design of cooling tower-technical guideline for the structural design,*

computation and execution of cooling towers (VGB-R 610Ue), BTR Bautechnik bei Kühltürmen, Essen.
Zhao, L. and Ge, Y.J. (2010), "Wind loading characteristics of super-large cooling towers", *Wind Struct.*, **13**(3), 257-273.

CC